

Simulation of Ultrasonic Stress During Impact Phase in Wire Bonding

Michael Mayer[†]

Microjoining Laboratory, Centre of Advanced Materials Joining, University of Waterloo, Canada

(Received December 20, 2013; Corrected December 24, 2013; Accepted December 26, 2013)

Abstract: As thermosonic ball bonding is developed for more and more advanced applications in the electronic packaging industry, the control of process stresses induced on the integrated circuits becomes more important. If Cu bonding wire is used instead of Au wire, larger ultrasonic levels are common during bonding. For advanced microchips the use of Cu based wire is risky because the ultrasonic stresses can cause chip damage. This risk needs to be managed by e.g. the use of ultrasound during the impact stage of the ball on the pad (“pre-bleed”) as it can reduce the strain hardening effect, which leads to a softer deformed ball that can be bonded with less ultrasound. To find the best profiles of ultrasound during impact, a numerical model is reported for ultrasonic bonding with capillary dynamics combined with a geometrical model describing ball deformation based on volume conservation and stress balance. This leads to an efficient procedure of ball bond modelling bypassing plasticity and contact pairs. The ultrasonic force and average stress at the bond zone are extracted from the numerical experiments for a 50 μm diameter free air ball deformed by a capillary with a hole diameter of 35 μm at the tip, a chamfer diameter of 51 μm , a chamfer angle of 90°, and a face angle of 1°. An upper limit of the ultrasonic amplitude during impact is derived below which the ultrasonic shear stress at the interface is not higher than 120 MPa, which can be recommended for low stress bonding.

Keywords: Wire Bond, Ultrasound, Underpad Stress

1. Introduction

Due to the high price of Au, the microelectronic wire bonding industry is making great efforts to adopt alternative wire materials that are more economical. In particular, Cu wire is used for ball bonding. In applications where Cu cannot be used yet, it is mainly due to the risk of chip damage due to the higher stresses during the Cu ball bonding process compared with the Au ball bonding processes. Copper is harder than Au and commonly needs larger levels of ultrasound and force for successful bonding. This causes higher stresses and thus higher risk of chip damage.

Various efforts were made to reduce stress in Cu wire bonding.¹⁻⁶⁾ One of them is to use ultrasound during impact, i.e. typically a reduced level of ultrasound amplitude during touchdown and initial deformation of the ball. This can reduce the work hardening effect of initial deformation.⁷⁻⁹⁾ The stress field under the bonding pad on a microchip can be measured during bonding only with very limited resolution¹⁰⁻¹³⁾ or after bonding with Raman measurements.¹⁴⁾ Therefore, several contributions used finite element modelling to better understand wire bonding.¹⁵⁻²¹⁾ Some contributions focus on

how ultrasonic stresses affect the microchip.¹⁵⁻²⁰⁾ While the main aspects of ball bonding were covered in these papers, simulations of the ultrasonic parameter during impact of the ball on the pad are scarce. Thus, a numerical method combined with a geometrical model is reported in this paper, describing how the free air ball (FAB) shape transforms in that of the deformed ball, as illustrated in Fig. 1, while calculating the ultrasonic force acting on the chip. This work is an extension of the extended abstract and presentation given previously.²²⁾

2. Geometric Model of Ball Deformation

The diameter of the FAB is 50 μm which is stepwise deformed by a capillary with a hole diameter of 35 μm at the tip, a chamfer diameter of 51 μm , a chamfer angle of 90°, and a face angle of 11°.

Models that incorporate plasticity need to handle contacts between components and both, plasticity and contact pairs need substantial calculation time. In contrast, the geometric model proposed here assumes all contacts are perfectly connected which corresponds to the ideal case where the

[†]Corresponding author
E-mail: mmayer@uwaterloo.ca

© 2013, The Korean Microelectronics and Packaging Society

This is an Open-Access article distributed under the terms of the Creative Commons Attribution Non-Commercial License(<http://creativecommons.org/licenses/by-nc/3.0>) which permits unrestricted non-commercial use, distribution, and reproduction in any medium, provided the original work is properly cited.

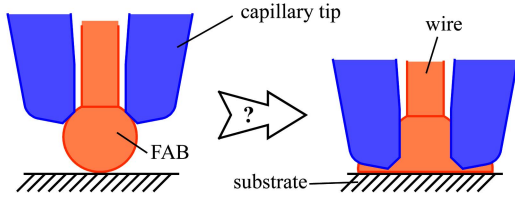


Fig. 1. Geometry variation during deformation of free-air ball (FAB).

ultrasound immediately bonds the interface and the normal (clamping) force is sufficiently high. These simplifications lead to a more robust and faster simulation. However, the results of this simplified model can only serve as an upper limit and any experimental values will be lower. This still allows to draw conclusions about recommended ranges of process parameters. Based on four concepts, this model describes the stepwise progress of ball formation by providing the deformed ball outline (shape) for each step. The model consists of two stages, the intrusion stage and the squeeze-out stage.

2.1. Intrusion Stage

Stepwise intrusion. In this concept, the capillary is moved downwards from the FAB touching position into the FAB by a specific distance d_z , e.g. $0.1 \mu\text{m}$. This intrusion is illustrated in the closeup in Fig. 2 (a). The normal force associated with this intrusion also acts at the ball/substrate contact zone, leading to a collapse of the initial point contact.

Stress balance. Inspired by Newton's third law of motion, not only the action and reaction forces are the same on the two interface areas, capillary/ball and ball substrate, but also the stresses as assumed the same in this model. Of course, this simplification is significant as the yield stresses depend on the part geometry and boundaries. The capillary/ball interface experiences friction and shear in a stronger way than the ball/substrate interface. Leaving a more accurate representation of this matter to future models, the simplification here means that the contact area, S_{tipcut} , is required to be the same as the area of the projection of the capillary/ball interface onto the substrate plane forming a ring, S_{ring} . From this follows the height of the cut off ball tip, g_z , and the total distance the capillary moves in this step, $d_z + g_z$.

Volume conservation. The volumes $V_{\text{intrusion}}$ and V_{tipcut} are moved to the periphery of the deformed ball by assuming the shape between capillary and substrate being that of the section of a circle with center point A having the same distance from the capillary point and substrate point, and a radius r adjusted for volume conservation, as shown in Fig.

2 (b). In cases of advanced deformation, e.g. when the distance of A from the axis of symmetry is larger than r , the auxiliary circle rotated around the axis of symmetry has the form of a donut.

2.2. Squeeze-Out Stage

In this stage the concept of stress balance is abandoned as it does not agree with experimental observation. It is replaced with an *exponential decline model* of point A. This position now follows the basic exponential function, bx

$$z = a \cdot e_{bx}, \quad (1)$$

where a and b are adjusted for each step while r remains constant. An example is shown in Fig. 3. The values of a and b are obtained by fitting Equ. 1 to the previous center point A and point C. The coordinates of C, x_C , y_C are constructed using the coordinates of the contact points of capillary/ball and substrate/ball, denoted E and D, with coordinates x_E , y_E and x_D , y_D , respectively, using

$$x_C = (x_E + x_D)/2 \quad (2)$$

$$y_C = (y_E + y_D)/4 \quad (3)$$

These formulas assure a deformed ball shape that is fairly similar to observed shapes. The formulas also assure that

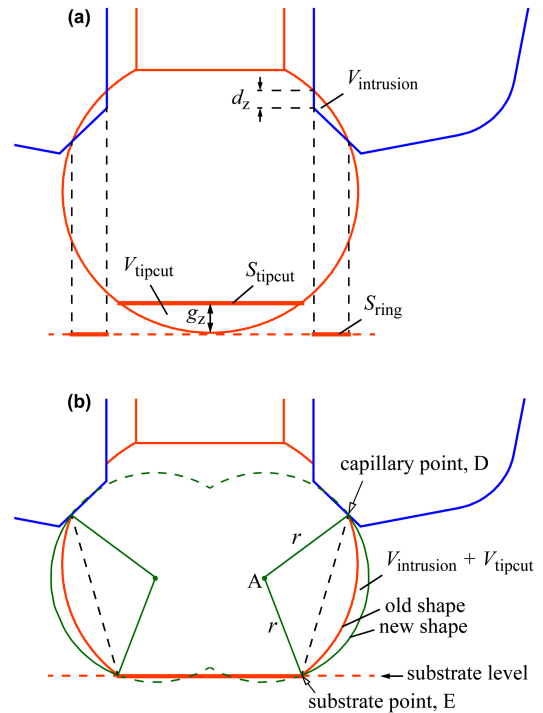


Fig. 2. Illustrations of (a) intrusion of capillary into ball where d_z is given and g_z is derived from the concept of stress balance, (b) new shape derived from concept of volume conservation by fitting a circle section between capillary and substrate, with point A as the circle center.

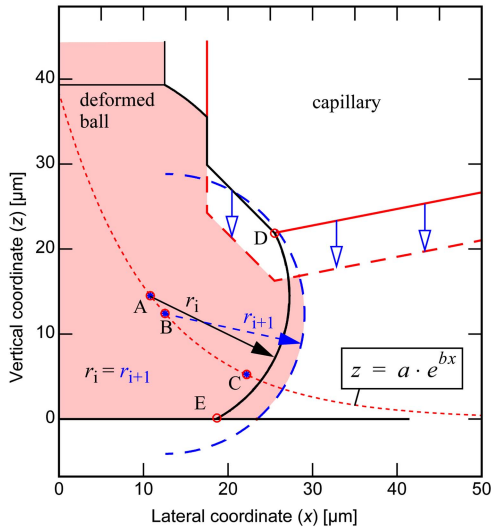


Fig. 3. Illustration of stage II construction. Position of B determined by concept of volume conservation while $r_i = r_{i+1}$ is kept constant.

the center point A manages to slip under the cap tip while the deformation is progressing to extreme values.

2.3. Example ball Deformation

Definitions of the geometry parameters of a deformed ball are given in Fig. 4. An example ball deformation run is carried out with initiating step sizes of $d_z = 0.01, 0.05,$ and then $0.1 \mu\text{m}$ for the rest of stage I, and $0.4 \mu\text{m}$ for stage II. The resulting values including the effect of gz are shown in Fig. 5. Examples of the geometries are given in Fig. 6. The geometry parameters for each step are given in Fig. 7.

3. Ultrasonic Finite Element Model

The same model as in⁽¹⁹⁻²¹⁾ for a Cu ball is used with the exception of the bonded ball geometry which is adjusted to various degrees of deformation while keeping the total

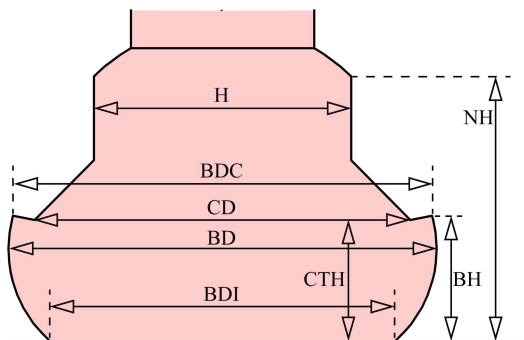


Fig. 4. Geometry parameters definitions for hole diameter H, neck height NH, chamfer diameter CD, ball diameter BD, ball diameters taken at capillary BDC and interface BDI, ball height BH, and capillary tip height CTH.

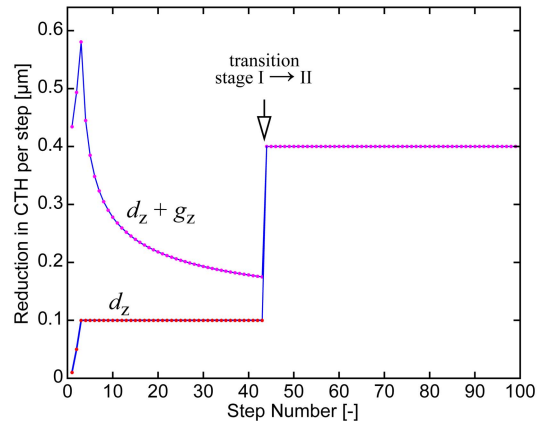


Fig. 5. Given (d_z) and derived ($d_z + g_z$) stepsize for example ball deformation by geometrical model.

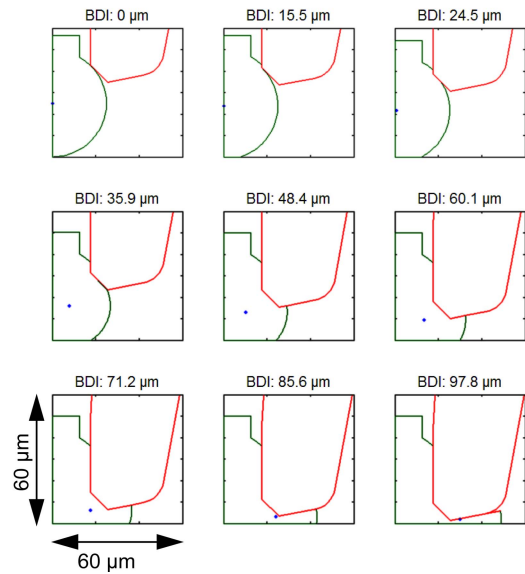


Fig. 6. Geometry variation examples ranging from ball height 21.5 micron down to 12.7 micron (only 1/2 model shown).

volume constant to be that of a 50 micron diameter FAB. For each of these geometries the stress field generated by ultrasound with a frequency of 128 kHz is simulated and the ultrasonic tangential force at the bond interface is determined. This force produces the ultra-sonic shear stress at the interface which usually cannot go above the shear strength of the best possible bond or of the base materials. For Au to Al or Cu to Al bonds, a shear strength of 120 MPa is reasonable.

Results for interfacial force and stress are shown in Figs. 8 (a) and (b), respectively. The stepsize was randomly chosen between $0.05 \mu\text{m}$ and $0.15 \mu\text{m}$ for each data point to visualize numerical noise. For increasing deformation, the stress is mainly decreasing. In other words, relatively high stresses can occur before deformation is finished provided the ultrasound is strong enough to cause bonding. The

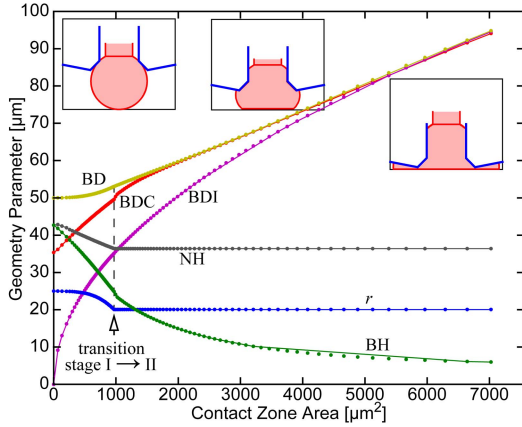


Fig. 7. Geometry parameters determined by the geometric deformation model.

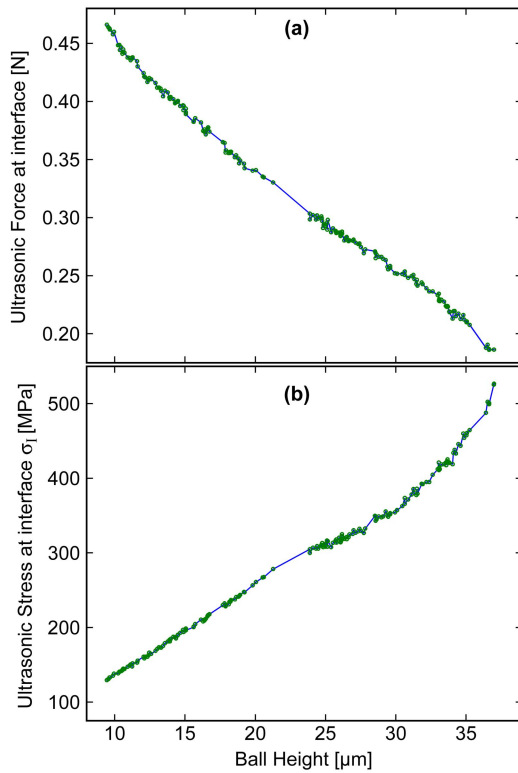


Fig. 8. Ultrasonic force (a), stress (b) at bond interface, dependent on ball deformation. Ultrasonic amplitude A_0 was 559 nm.

number of mesh elements used depends on the geometry and varies between 16000 and 19000.

To make sure there is no ultrasound induced failure during impact, we assume the interfacial ultrasonic stress need to be always below a limit of $\sigma_{\text{Target}} = 120$ MPa, the ultrasonic amplitude must be lowered below a limit,

$$A_{\text{Limit}} = A_0 \cdot \sigma_{\text{Target}} / \sigma_1, \quad (4)$$

where A_0 is the horn amplitude used in the simulation,

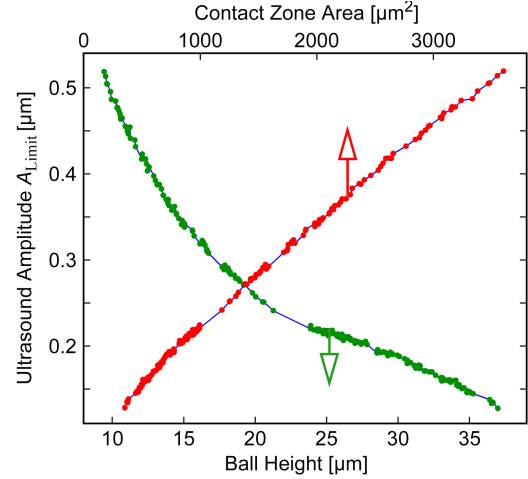


Fig. 9. Upper limit of ultrasonic amplitude to avoid ultrasonic stress levels above 120 MPa at interface.

0.599 mm, and σ_1 is the resulting interfacial ultrasonic stress. The result of this derivation is shown in Fig. 9. The A_{Limit} value is roughly linear with the contact zone area.

4. Conclusions

A geometrical model is reported that predicts the progressive free air ball deformation purely based on the starting geometry of free air ball and capillary tip. Based on four simplifying concepts, the model produces deformed ball shapes that correspond well with experimentally observed ball shapes. A finite element model is used on the progressing geometries to estimate ultrasonic stress levels at the interface in ball bonding during impact formation with pre-bleed ultrasound. A significant change in ultrasonic effect is observed depending on the amount of ball deformation.

The model can be used to estimate optimized ultrasound profiles during the initial deformation of balls and thereby can lead to processes with minimized risk of underpad damage. The model lends itself to extension, e.g. for various capillary geometries or for non-spherical FAB shapes, and for analysis of process sensitivity to parameter variations, e.g. of the capillary tip parameters (hole, chamfer) or the free air ball diameter.

Acknowledgement

This work is supported by the Natural Science and Engineering Research Council (NSERC) of Canada, and the Initiative for Automotive Manufacturing Innovation (IAMI), Ontario, Canada.

References

1. Rezvani, A., Mayer, M., Shah, A., Zhou, N., Hong, S.J., Moon, J. T., "Free-air ball formation and deformability with Pd coated Cu wire", Proceedings - Electronic Components and Technology Conference, art., 5898711, 1516 (2011).
2. Shah, A., Rezvani, A., Mayer, M., Zhou, Y., Persic, J., Moon, J.T., "Reduction of ultrasonic pad stress and aluminum splash in copper ball bonding", Microelectronics Reliability, 51(1), 67 (2011).
3. Qin, I., Shah, A., Huynh, C., Meyer, M., Mayer, M., Zhou, Y., "Effect of process parameters on pad damage during Au and Cu ball bonding processes", Proceedings of the Electronic Packaging Technology Conference, EPTC, art., 5416482, 573 (2009).
4. Shah, A., Mayer, M., Zhou, Y., Persic, J., Moon, J.T., "Optimization of ultrasound and bond force to reduce pad stress in thermosonic Cu ball bonding, Proceedings of the Electronic Packaging Technology Conference", EPTC, art., 5416580, 10 (2009).
5. Shah, A., Mayer, M., Zhou, Y.N., Hong, S.J., Moon, J.T., "Low-stress thermosonic copper ball bonding, IEEE Transactions on Electronics Packaging Manufacturing", 32(3), 176 (2009).
6. Shah, A., Mayer, M., Zhou, Y., Hong, S.J., Moon, J.T., "Reduction of underpad stress in thermosonic copper ball bonding", Proceedings - Electronic Components and Technology Conference, art.,4550279, 2123 (2008).
7. Huang, H., Pequegnat, A., Chang, B.H., Mayer, M., Du, D., Zhou, Y., "Influence of superimposed ultrasound on deformability of Cu", Journal of Applied Physics, 106(11), (2009).
8. Lum, I., Hang, C.J., Mayer, M., Zhou, Y., "In situ studies of the effect of ultrasound during deformation on residual hardness of a metal", Journal of Electronic Materials, 38(5), 647 (2009).
9. Lum, I., Huang, H., Chang, B.H., Mayer, M., Du, D., Zhou, Y., "Effects of superimposed ultrasound on deformation of gold, Journal of Applied Physics", 105(2), 024905, (2009).
10. Mayer, M., Paul, O., Baltès, H., "In-situ measurement of stress and temperature under bonding pads during wire bonding using integrated microsensors", Proc. 2nd Int. Conf. Emerging Microelectr. and Interconn. Technol. EMIT, 98, 129 (1998).
11. Doelle, M., Peters, C., Ruther, P., Paul, O., "Piezo-FET stress-sensor arrays for wire-bonding characterization", Microelectromechanical Systems, 15(1), 120 (2006).
12. Mayer, M., J. T. Moon, and J. Persic. "Measuring stress next to Au ball bond during high temperature aging", Microelectronics Reliability, 49(7), 771 (2009).
13. Lemke, B., Baskaran, R., Paul, O., "Piezoresistive CMOS sensor for the localized measurement of five independent stress components", Micro Electro Mechanical Systems (MEMS), 2010 IEEE 23rd International Conference on, pp. 596-599. IEEE, (2010).
14. Chen, J., Degryse, D., Ratchev, P., De Wolf, I., "Mechanical issues of Cu-to-Cu wire bonding." Components and Packaging Technologies, IEEE Transactions on 27(3), 539 (2004).
15. Degryse, D., Vandeveld, B., Beyne, E., "Mechanical FEM simulation of bonding process on Cu LowK wafers", Components and Packaging Technologies, IEEE Transactions on 27(4), 643 (2004).
16. Liu, Y., Irving, S., Timwah Luk. "Thermosonic wire bonding process simulation and bond pad over active stress analysis", Electronics Packaging Manufacturing, IEEE Transactions on 31(1), 61 (2008).
17. Wright, A., Koffell, S., Pichler, P., Enichlmair, H., Minixhofer, R., Wachmann, E., "On the Thermo-Mechanical Modelling of a Ball Bonding Process with Ultrasonic Softening", Proc. IEEE EuroSimE conference, (2013).
18. Lin, H. Y., Upreti, K., Tippmann, A., Subbarayan, G., Jung, D. Y., Sammakia, B., "Simulations of Deformation and Stress During Copper Wirebond on ULK Chips", Proc. of ASME InterPACK2013 conference, (2013).
19. Huang, Y., Mayer, M., "Effects of ultrasonic capillary dynamics and pad material on the mechanics of thermosonic ball bonding", Proceedings - IEEE Ultrasonics Symposium, art., 5441817, (2009).
20. Huang, Y., Shah, A., Mayer, M., Zhou, N., Persic, J., "Effect of ultrasonic capillary dynamics on the mechanics of thermosonic ball bonding", IEEE Transactions on Ultrasonics, Ferroelectrics, and Frequency Control, 57(1), art., no. 5361546, 241 (2010).
21. Mayer, M., Huang, Y., "Numerical analysis of ultra-high frequency wire bonding", Proc. International Symposium on Microelectronics, IMAPS 2009, 388 (2009).
22. Mayer, M., "Ultrasonic Stresses in Copper Wire Bonding with Pre-Bleed Ultrasound", extended abstract and presentation, 1st International Conference for Nanojoining and Microjoining, Beijing, China, (2012).